J. Appl. Comput. Mech., 6(2) (2020) 183-199
DOI: 10.22055/JACM.2019.28695.1498

ISSN: 2383-4536
jacm.scu.ac.ir

M&MoCS
Shahid Chamran University of Ahvaz

Journal of
Applied and Computational Mechanics

Research Paper

Viscoelastic Micropolar Convection Flows from an Inclined Plane with Nonlinear Temperature: A Numerical Study

S. Abdul Gaffar[1], P. Ramesh Reddy[2], V. Ramachandra Prasad[3], A. Subba Rao[4]
B. Md. Hidayathulla Khan[5]

[1] Department of Information Technology, Mathematics Section, Salalah College of Technology
Salalah -211, Oman, Email: sa.gaffar@sct.edu.om

[2] Department of Mathematics, Madanapalle Institute of Technology & Science
Madanapalle - 517325, India, Email: prreddy.mits@gmail.com

[3] Department of Mathematics, School of Advanced Sciences, Vellore Institute of Technology
Vellore – 632014, India, Email: rcpmaths@gmail.com

[4] Department of Mathematics, Madanapalle Institute of Technology & Science
Madanapalle - 517325, India, Email: prreddy.mits@gmail.com

[5] Department of Mathematics, Sir Vishveshwaraiah Institute of Science and Technology
Madanapalle – 517325, India, Email: bmdhkh@gmail.com

Received February 21 2019; Revised May 05 2019; Accepted for publication May 12 2019.
Corresponding author: S. Abdul Gaffar (sa.gaffar@sct.edu.om)

Abstract. An analytical model is developed to study the viscoelastic micropolar fluid convection from an inclined plate as a simulation of electro-conductive polymer materials processing with nonlinear temperature. Jeffery's viscoelastic model is deployed to describe the non-Newtonian characteristics of the fluid and provides a good approximation for polymers. Micro-structural is one of the characteristics of non-Newtonian fluid that represents certain polymers, which constitutes a novelty of the present work. The normalized nonlinear boundary value problem is solved computationally with the Keller-Box implicit finite-difference technique. Extensive solutions for velocity, surface temperature, angular velocity, skin friction, heat transfer rate and wall couple stress are visualized numerically and graphically for various thermophysical parameters. Validation is conducted with earlier published work for the case of a vertical plate in the absence of viscous dissipation, chemical reaction and non-Newtonian effects. This particle study finds applications in different industries like reliable equipment design, nuclear plants, paint spray, thermal fabrication, water-based gel solvents, polymeric manufacturing process, gas turbines and different propulsion devices.

Keywords: Viscoelastic fluid, Micropolar Fluid, Nonlinear Temperature, Retardation time, Vorticity.

1. Introduction

The transport phenomena along an inclined surface arise in many applications in industry such as fuel combustion [1], condensation systems [2], magnetic thin film deposition [3], geophysical debris flows [4], thermal coating [5] and geothermal heat transfer from oblique faults [6]. In materials processing systems, the use of an inclined plane allows the thermal buoyancy force to easily modify as it is proportional to the inclination angle. Materials manufacturing operations (e.g. plastic coating dynamics [7], gel and thin film systems [8]) also feature non-Newtonian fluids. Rheology of the involved fluids significantly modifies momentum and heat transfer characteristics in such flows. In the context of

Published online: August 22 2019

thermoplastic sheet processing, viscoelastic film flows may become unstable due to fluid elasticity which is controlled by the Weissenberg number [9]. Many rheological models have subsequently been deployed in recent years to study thermal and momentum boundary-layer flows from inclined surfaces. These studies have also utilized many advanced numerical methods which are required to accommodate the nonlinearity of such flows. Ilias and Rawi [10] used the incompressible ferrofluid model and Keller-Box method to investigate the MHD convection boundary layer flow from an inclined plate. They observed that the temperature enhances with an increase in the inclination angle. Kandasamy *et al.* [11] numerically investigated the effects of particle shape of radiative MHD water-based nanofluid past a nonlinear inclined surface. Khan *et al.* [12] analyzed the MHD mixed convection boundary layer flows past an inclined surface using homotopy analysis method. They observed a significant increase in heat and mass transfer boundary layer with an increase in the Lewis number. Prasad *et al*. [13] presented the radiative MHD mixed convection flow of Casson fluid past an infinite inclined plate with thermal diffusion using finite element method. They observed that the Casson fluid, magnetic and inclination angle parameters decelerate the boundary layer flow. Shamshuddin *et al*. [14] used the Casson fluid and Galerkin finite element method to investigate the chemically radiative MHD convection flows from an inclined porous plate. They observed a decrease in flow with a decrease in the inclination angle and an increase in thermal boundary layer flow. Few recent studies include, power-law fluid flows [15], nanofluid flows [16], third grade fluid flows [17], Williamson fluid flows [18], Maxwell fluid flows [19], Powell-Eyring Magneto-Nanofluid flows [20], Upper-Convected Maxwell Fluid fluids [21], Eyring Powell Nanofluid flows with chemical reaction [22], Williamson nanofluid flows over a Riga plate with chemical reaction [23] and micropolar fluid flows [24]. Among the many viscoelastic fluids available, Jeffrey model [25] has emerged as a good approximation for polymer dynamics. This model features three constants, namely the zero shear-rate viscosity, ratio of relaxation and retardation time and the retardation time. It is appropriate for nonlinear viscoelastic effects for which the simpler inelastic models cannot be used. Jeffrey's model is obtained by adding a time derivative of the shear rate to the conventional Maxwell linear model. The convected Jeffrey model (Oldroyd model) also allows several other special cases to be obtained. When retardation time is neglected the original Maxwell model is retrieved. When the relaxation time is neglected then the case of a second order differential fluid is obtained for which the normal stress coefficient is zero. Finally, when both relaxation and retardation times are equivalent, then the Newtonian fluid case is obtained. Jeffrey's model was used by Prasad *et al.* [26] to study steady-state thermal polymer coating flow of a plate in porous media. Gaffar *et al.* [27] investigated the non-isothermal and non-isolutal transport phenomena from a porous conical body using Jeffrey's model. These studies all showed how significant modifications are computed in heat, flow and species diffusion fields due to viscoelastic material behavior. Ahmad and Ishak [28] studied the steady magnetohydrodynamic flow of Jeffrey fluid from a stretching vertical surface using an implicit finite difference method. They showed that increasing Jeffrey fluid parameters (relaxation and retardation parameters) reduce skin friction whereas the contrary effect is induced with a stronger magnetic field.

The micro-structural features of the fluid have been neglected in the rheology's discusses above. Numerous polymers involve complex suspensions of a mind boggling nature which cannot be dissected adequately precisely with viscoelastic models. To suit this disparity in non-Newtonian models, Eringen [29], in the 1960s, developed the microcontinuum fluid mechanics that presents the thermodynamics of micro-structure that have different applications in industry and nature such as gyratory motions, spin, couple stresses, etc. A simple version of micro-morphic fluid termed as *micropolar fluid* have been developed by Eringen [30]. The micropolar fluid exhibits microscopic effects due to local structure and micro-motions of fluid elements. Eringen [31] further developed the thermos-micropolar fluid theory. Mishra *et al.* [32] studied the influence of radiative flux on micropolar fluid in transient magnetized flow with heat source from a semi-infinite horizontal plate using shooting technique. Igor and Marko [33] made an extensive investigation on micropolar fluid flows through a thin pipe with a constant circular cross-section. Nazeer *et al.* [34] investigated the effects of magnetohydrodynamic parameter on the natural convection boundary layer flow of micropolar fluid in a porous container using finite element technique. Koriko *et al.* [35] showed that thermal stratification reduces temperatures and reduces micro-rotation profiles in magnetic micropolar fluid flow along a vertical surface with binary chemical reaction. Rashid *et al.* [36] observed that micro-rotation profiles increase with Hartman number in micropolar fluid flow of two horizontal parallel plates in a rotating system using optimal homotopy analysis method. Ramzan *et al*. [37] numerically investigated the flows of micropolar nanofluid over a rotating disk with slip and magnetic field effects. They observed that increasing magnetic field effects decelerates velocity and microrotation whereas accelerates both temperature and concentration profiles. Ramzan *et al*. [38] developed a mathematical model to examine the magnetohydrodynamic micropolar nanofluid flow in the presence of nonlinear radiation, dual stratification, and chemical reaction.

In recent years new sophisticated *polymers* have emerged which provide enhanced performance in many industrial sectors including aerospace, manufacturing, energy and medical engineering. These include magnetoelectric nanocomposites [39] and soft magnetic polymer gels [40]. These materials are frequently synthesized at high temperature. The current study therefore aims to simulate the transport phenomena in the flow of such materials along an inclined surface within micropolar fluid regime with nonlinear temperature. Jeffrey's rheological model is deployed for non-Newtonian behavior. The emerging non-dimensional nonlinear boundary value problem is solved with the Keller box implicit finite difference method [41 – 44]. Verification of the computations is included via comparison with earlier studies. Extensive visualization via graphs of the influence of key parameters (*Deborah viscoelastic parameter*, *the ratio of relaxation to retardation parameter, Micropolar parameter, micro-inertia density parameter, inclination angle, mixed convection parameter, nonlinear temperature parameter*, etc.) on velocity, temperature, skin friction, heat and mass transfer rate characteristics is included. The present problem to the authors' knowledge has not been considered in the scientific literature and constitutes a novel effort in thermodynamic analysis of magnetic non-Newtonian materials processing operations.

2. Micropolar Constitutive Model

This section presents the viscoelastic properties of the polymer of the rheological model considered in the present study. Actually, polymers are suspensionable and can be rotated and also get deformed. A micro-continuum model is necessary to mimic the micro-structural properties. The Eringen's micropolar model [29] is a versatile and compatible polymeric flow model and is the simplified form of the more general micro fluid model [30]. The micropolar fluid behaves and exhibits properties of the microelements which possess local inertia. Micropolar fluids contain non-deformable rigid particles called volume elements and are defined by a micro-rotation vector. In micropolar fluid mechanics, the classical continuum laws are augmented with additional equations which account for the conservation of micro-inertia moments and the balance of first stress moments which arise due to the micro-structure in the fluid. Thereby the kinematic variables (gyration tensor, micro-inertia moment tensor) and the concepts of body moments, stress moments and microstresses are combined with classical continuum fluid dynamics theory. The momentum field equations for micropolar fluid in generalized form are as follows [45 – 46]:
Linear Momentum:

$$(\lambda_2+2\mu+k)\nabla\nabla\bullet V-(\mu+k)\nabla\times\nabla\times V+k\nabla\times G-\nabla P+\rho f=\rho V' \tag{i}$$

Angular Momentum:

$$\left(\alpha^*+\beta^*+\gamma\right)\nabla\nabla\bullet G-\gamma\nabla\times\nabla\times G+k\nabla\times V-2kG+\rho l=\rho jG' \tag{ii}$$

where ρ is *mass density of the micropolar fluid, V is* the translational velocity vector, G is angular velocity vector, j is microinertial density, ***f*** is the body force per unit mass vector. Also, ***l*** is the body couple per unit mass vector, p is the thermodynamic pressure, μ is the Newtonian dynamic viscosity, λ_2 is the Eringen second order viscosity coefficient, k is the vortex viscosity coefficient and α^*, β^* and γ are spin gradient viscosity coefficients for micropolar fluids. In micropolar model we are confined to only two independent kinematical vector fields, viz., the velocity vector field and the axial vector field which simulates the spin or the micro-rotations of the micropolar fluid particles, which are assumed to be rigid. In the theory of micropolar fluid for unsteady flows, no external forces exist and for steady flows, the conservation equations are simplified.

3. Mathematical Model

Natural convection in laminar, two-dimensional, time-independent incompressible Jeffrey viscoelastic polymer flow from an inclined rigid sheet in micropolar fluid regime with nonlinear temperature is considered, as illustrated in Fig. 1. The sheet is inclined at an angle, Ω, to the horizontal. The polymer is assumed to be an optically dense, absorbing but non-scattering fluent medium. In this model, with the exception of the density variation in the buoyancy terms (Boussinesq approximation) all other properties are assumed to be constant. To simulate non-Newtonian characteristics of Jeffery's elastic-viscous fluid model, the Cauchy stress tensor is required which is defined as:

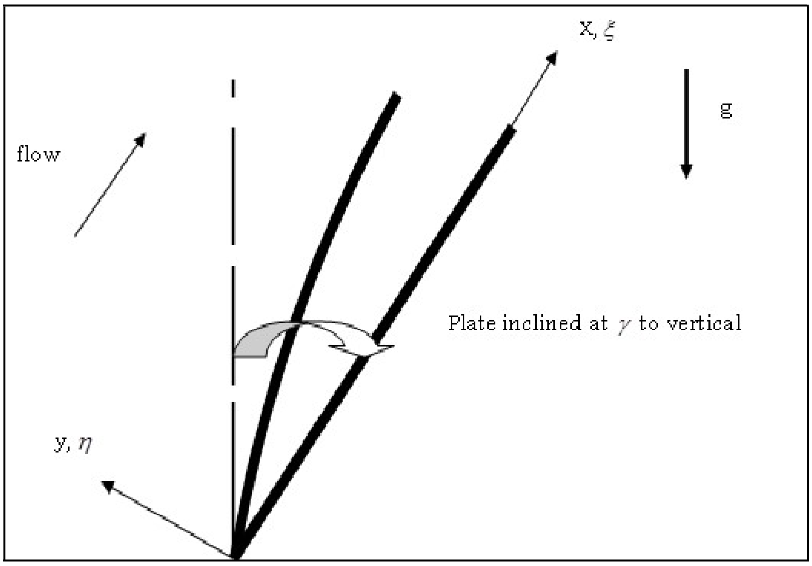

Fig. 1. Physical model for inclined plane flow

$$T=-pI+S,\ S=\frac{\mu}{1+\lambda}\left(\dot{\gamma}+\lambda_1\ddot{\gamma}\right) \tag{1}$$

$$\dot{\gamma}=\nabla V+(\nabla V)^t \tag{2}$$

$$\ddot{\gamma}=\frac{d}{dt}\left(\dot{\gamma}\right) \tag{3}$$

Here, p, I, S, μ, λ, λ_1 and $\dot{\gamma}$, denote pressure, identity tensor, Cauchy stress tensor for *Jeffery fluid*, viscosity, ratio of relaxation to retardation time, retardation time and shear rate, respectively. Jeffery's model therefore features three constants i.e. viscosity at zero shear rate and two time-related material parameter constants. In line with [25-21, 45] (for Jeffrey's fluid) and Beg *et al*. [46 – 47] (for micropolar fluid) and incorporating the appropriate terms under the boundary-layer approximation, the following conservation equations emerge for mass, momentum, energy (heat) and concentration:

$$\frac{\partial u}{\partial x}+\frac{\partial u}{\partial y}=0 \tag{4}$$

$$\begin{aligned}\rho\left(u\frac{\partial u}{\partial x}+v\frac{\partial u}{\partial y}\right)=\frac{\mu+k}{1+\lambda}\frac{\partial^2 u}{\partial y^2}+\frac{\mu\lambda_1}{1+\lambda}\left(u\frac{\partial^3 u}{\partial x\partial y^2}+\frac{\partial u}{\partial x}\frac{\partial^2 u}{\partial y^2}+\frac{\partial u}{\partial y}\frac{\partial^2 u}{\partial x\partial y}+v\frac{\partial^3 u}{\partial y^3}\right)+k\frac{\partial N}{\partial y}\\ +\rho g_1\left(\beta_0\left(T-T_\infty\right)+\beta_1\left(T-T_\infty\right)^2\right)\cos\Omega\end{aligned} \tag{5}$$

$$\rho j\left(u\frac{\partial N}{\partial x}+v\frac{\partial N}{\partial y}\right)=\gamma\frac{\partial^2 N}{\partial y^2}-k\left[2N+\frac{\partial u}{\partial y}\right] \tag{6}$$

$$u\frac{\partial T}{\partial x}+v\frac{\partial T}{\partial y}=\frac{k}{\rho c_p}\frac{\partial^2 T}{\partial y^2} \tag{7}$$

where u and v are the velocity components in the x and y directions, respectively, $\gamma=(\mu+[k/2])j$ is the gyro-viscosity (shear spin) of micropolar fluid and all the other terms are defined in the nomenclature. The relevant boundary conditions imposed at the plate surface and in the free stream are as:

$$\begin{aligned}&\text{at}\quad y=0,\quad u=0,\quad v=0,\quad N=-\frac{1}{2}\frac{\partial u}{\partial y},\quad T=T_w\\ &\text{when}\quad y\to\infty,\quad u\to u_\infty,\quad v\to 0,\quad N\to 0,\quad T\to T_\infty\end{aligned} \tag{8}$$

The nonlinearity of the conservation equations in primitive variables makes even a numerical solution difficult. It is judicious therefore to reduce the number of independent variables and to this end the following group of variables is invoked:

$$\xi=\frac{x}{L},\quad \eta=y\left(\frac{u_\infty}{\nu x}\right)^{1/2},\quad \psi=\left(\nu u_\infty x\right)^{1/2}f,\quad \theta(\xi,\eta)=\frac{T-T_\infty}{T_w-T_\infty},\quad g=\frac{LN}{u_\infty}\left(\frac{\xi}{\mathrm{Re}}\right)^{1/2} \tag{9}$$

Introducing the stream function ψ defined as $u=\partial\psi/\partial y$ and $v=-\partial\psi/\partial x$. Incorporating Eqn. (9) into Eqns. (4) - (7), the continuity equation (4) is automatically satisfied and the emerging non-dimensional momentum and thermal boundary layer equations emerge as:

$$\begin{aligned}\frac{1+K}{1+\lambda}f'''+\frac{1}{2}ff''+R\xi\theta\left(1+\alpha_1\theta\right)\cos\Omega+K\,g'-\frac{\mathrm{De}}{1+\lambda}\left(\frac{1}{2}f''^2+f'f'''+\frac{1}{2}ff^{iv}\right)\\ =\xi\left(f'\frac{\partial f'}{\partial\xi}-f''\frac{\partial f}{\partial\xi}-\frac{\mathrm{De}}{1+\lambda}\left(f'\frac{\partial f'''}{\partial\xi}-f'''\frac{\partial f'}{\partial\xi}+f''\frac{\partial f''}{\partial\xi}-f^{iv}\frac{\partial f}{\partial\xi}\right)\right)\end{aligned} \tag{10}$$

$$\left(1+\frac{K}{2}\right)g''+\frac{1}{2}fg'+\frac{1}{2}f'g-BK\xi\left[2g+f''\right]=\xi\left(f'\frac{\partial g}{\partial\xi}-g'\frac{\partial f}{\partial\xi}\right) \tag{11}$$

$$\frac{\theta''}{\Pr}+\frac{1}{2}f\theta'=\xi\left(f'\frac{\partial\theta}{\partial\xi}-\theta'\frac{\partial f}{\partial\xi}\right) \tag{12}$$

The transformed dimensionless wall and free stream boundary conditions assume the form:

$$\begin{aligned}&\text{at}\quad \eta=0,\qquad f=0,\quad f'=0,\quad g=-\frac{1}{2}\frac{\partial^2 f}{\partial y^2},\quad \theta=1\\&\text{when}\quad \eta\to\infty,\quad f'\to 1,\quad f''\to 0,\quad g\to 0,\quad \theta\to 0\end{aligned} \tag{13}$$

where

$$\begin{aligned}&De=\frac{\lambda_1\nu\,\mathrm{Re}_x}{x^2},\quad \mathrm{Re}_x=\frac{u_\infty x}{\nu},\quad Re=\frac{u_\infty L}{\nu},\quad Gr=\frac{g_1\beta(T_w-T_\infty)L^3}{\nu^2}\\&Ri=\frac{Gr}{\mathrm{Re}^2},\quad \Pr=\frac{\nu\rho c_p}{k},\quad B=\frac{L^2}{j\,\mathrm{Re}},\quad K=\frac{k}{\mu},\quad \alpha_1=\frac{\beta_1(T_w-T_\infty)}{\beta_0}\end{aligned} \tag{14}$$

Additionally, the dimensionless expressions for the physical quantities at the plate surface can be written as:

$$\sqrt{\mathrm{Re}_x}C_f=\frac{1+K}{1+\lambda}f'''(\xi,0)-\frac{De}{2(1+\lambda)}\left[f'(\xi,0)*f''(\xi,0)+f(\xi,0)*f'''(\xi,0)\right] \tag{15}$$

$$M_w=g'(\xi,0) \tag{16}$$

$$\frac{Nu}{\sqrt{\mathrm{Re}_x}}=-\theta'(\xi,0) \tag{17}$$

Here the expressions $\sqrt{\mathrm{Re}_x}\,C_f, M_w$ and $Sh/\sqrt{\mathrm{Re}_x}$ denote skin friction coefficient (wall shear stress function), wall couple stress and local Nusselt number (wall heat transfer rate), respectively.

4. Numerical Finite Difference Solution

The boundary value problem to be solved comprises Eqs. (10) - (12) under boundary conditions (13). The Keller box method is selected to obtain numerical solutions. This method is well-documented in many studies [48 – 51] and details are therefore omitted here. This technique has remained extremely popular and maintained comparable efficiency to other numerical methods. The Keller-Box technique has second-order accuracy with arbitrary spacing and attractive extrapolation features. This numerical technique is very stable and exceptional accuracy is achieved. The Keller-Box method converges quickly and provides stable numerical meshing features. This method provides an improvement in accuracy on explicit or semi-implicit schemes and utilizes customizable stepping in a fully implicit approach. The Keller-Box discretization is fully coupled at each step which reflects the physics of parabolic systems. The discrete calculus of the Keller-Box technique is fundamentally different from all other numerical techniques. The Keller-Box technique comprises of four stages:

1. Decomposition of the N^{th} order partial differential equation system to N first-order equations.
2. Finite difference discretization
3. Quasilinearization of Non-Liner Keller Algebraic Equations.
4. Block-tridiagonal elimination.

Step 1: Decomposition of the N^{th} order partial differential equation system to N first order equations

The following new variables are introduced in Eqs. (10) – (13), to render the boundary value problem as a multiple system of first order equations.

$$u(x,y)=f',\ v(x,y)=f'',\ q(x,y)=f''',g(x,y)=p,s(x,y)=\theta,\ t(x,y)=\theta' \tag{18}$$

$$f'=u \tag{19}$$

$$u'=v \tag{20}$$

$$v'=q \tag{21}$$

$$g' = p \tag{22}$$

$$s' = t \tag{23}$$

$$\begin{aligned}\frac{1+K}{1+\lambda}v' + \frac{1}{2}fv + R\xi s(1+\alpha_1 s)\cos\Omega + Kp - \frac{\text{De}}{1+\lambda}\left(\frac{1}{2}v^2 + uq + \frac{1}{2}fv'\right) \\ = \xi\left(u\frac{\partial u}{\partial \xi} - v\frac{\partial f}{\partial \xi} - \frac{\text{De}}{1+\lambda}\left(u\frac{\partial q}{\partial \xi} - q\frac{\partial u}{\partial \xi} + v\frac{\partial v}{\partial \xi} - v'\frac{\partial f}{\partial \xi}\right)\right)\end{aligned} \tag{24}$$

$$\left(1+\frac{K}{2}\right)p' + \frac{1}{2}fp + \frac{1}{2}ug - BK\xi[2g+v] = \xi\left(u\frac{\partial g}{\partial \xi} - p\frac{\partial f}{\partial \xi}\right) \tag{25}$$

$$\frac{t'}{\text{Pr}} + \frac{1}{2}ft = \xi\left(u\frac{\partial s}{\partial \xi} - t\frac{\partial f}{\partial \xi}\right) \tag{26}$$

Here primes indicate differentiation w.r.t. η. Hence, the boundary conditions are:

$$\begin{aligned}&\text{at} \quad \eta = 0, \quad f = 0, \quad u = 0, \quad g = -\frac{1}{2}v, \quad s = 1 \\ &\text{when} \quad \eta \to \infty, \quad u \to 1, \quad v \to 0, \quad g \to 0, \quad s \to 0\end{aligned} \tag{27}$$

Step 2: Finite Difference Discretization

A 2-D computational grid is imposed on the ξ-η plane as shown in Fig. 2. The stepping process is as given below:

$$\begin{aligned}&\eta_0 = 0, \quad \eta_j = \eta_{j-1} + h_j, \quad j = 1,2,\ldots,J, \quad \eta_J = \eta_\infty \\ &\xi^0 = 0, \quad \xi^n = \xi^{n-1} + k_n, \quad n = 1,2,\ldots,N\end{aligned} \tag{28}$$

where k_n is the $\Delta\xi$ - spacing and h_j is the $\Delta\eta$ - spacing.

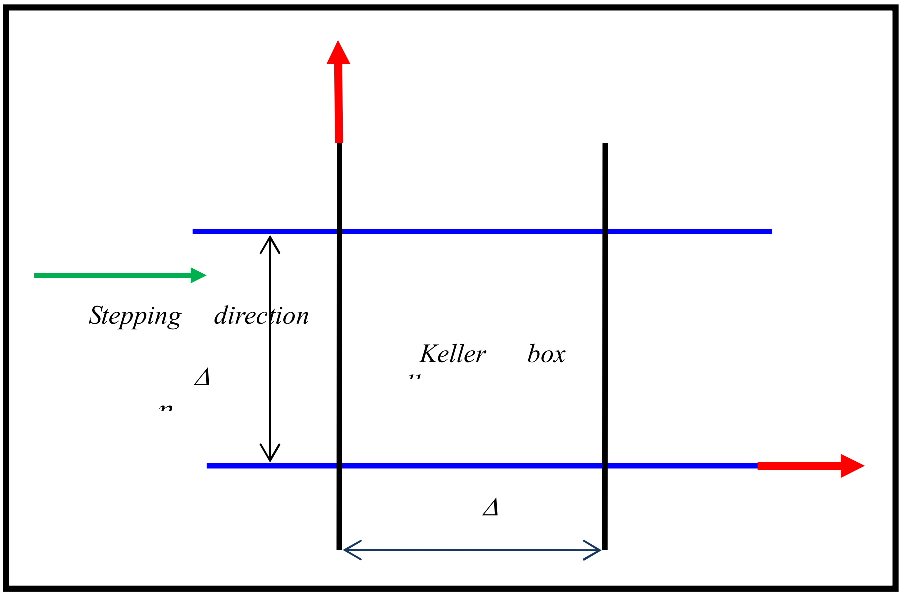

Fig. 2. Keller box computational cell

If g_j^n denotes the value of any variable at (η_j, ξ^n), then the variables and derivatives of Equations (19) – (26) at $(\eta_{j-1/2}, \xi^{n-1/2})$ are replaced by:

$$g_{j-1/2}^{n-1/2} = \frac{1}{4}\left(g_j^n + g_{j-1}^n + g_j^{n-1} + g_{j-1}^{n-1}\right) \tag{29}$$

$$\left(\frac{\partial g}{\partial \eta}\right)_{j-1/2}^{n-1/2}=\frac{1}{2h_j}\left(g_j^n-g_{j-1}^n+g_j^{n-1}-g_{j-1}^{n-1}\right) \tag{30}$$

$$\left(\frac{\partial g}{\partial \xi}\right)_{j-1/2}^{n-1/2}=\frac{1}{2k^n}\left(g_j^n-g_{j-1}^n+g_j^{n-1}-g_{j-1}^{n-1}\right) \tag{31}$$

The resulting finite - difference approximation of equations (19) – (26) for the mid-point $(\eta_{j-1/2},\xi^n)$, are:

$$h_j^{-1}\left(f_j^n-f_{j-1}^n\right)=u_{j-1/2}^n \tag{32}$$

$$h_j^{-1}\left(u_j^n-u_{j-1}^n\right)=v_{j-1/2}^n \tag{33}$$

$$h_j^{-1}\left(v_j^n-v_{j-1}^n\right)=q_{j-1/2}^n \tag{34}$$

$$h_j^{-1}\left(g_j^n-g_{j-1}^n\right)=p_{j-1/2}^n \tag{35}$$

$$h_j^{-1}\left(s_j^n-s_{j-1}^n\right)=t_{j-1/2}^n \tag{36}$$

$$\begin{aligned}&\frac{1+K}{1+\lambda}\left(v_j-v_{j-1}\right)+\left(\frac{1}{2}+\alpha\right)\frac{h_j}{4}\left(f_j+f_{j-1}\right)\left(v_j+v_{j-1}\right)-\frac{\mathrm{De}}{1+\lambda}\frac{h_j}{4}\left(u_j+u_{j-1}\right)\left(q_j+q_{j-1}\right)\\&-\frac{\mathrm{De}}{1+\lambda}\left(\frac{1}{2}-\alpha\right)\frac{h_j}{4}\left(v_j+v_{j-1}\right)^2-\frac{\mathrm{De}}{1+\lambda}\left(\frac{1}{2}+\alpha\right)\frac{1}{2}\left(f_j+f_{j-1}\right)\left(q_j-q_{j-1}\right)+R\xi\frac{h_j}{2}\left(s_j+s_{j-1}\right)\cos\Omega\\&+R\xi\frac{h_j}{4}\left(s_j+s_{j-1}\right)^2\alpha_1\cos\Omega+K\frac{h_j}{2}\left(p_j+p_{j-1}\right)-\alpha\frac{h_j}{4}\left(u_j+u_{j-1}\right)^2-\alpha\frac{h_j}{2}f_{j-1/2}^{n-1}\left(v_j+v_{j-1}\right)\\&+\alpha\frac{h_j}{2}v_{j-1/2}^{n-1}\left(f_j+f_{j-1}\right)+\alpha\frac{\mathrm{De}}{1+\lambda}h_ju_{j-1/2}^{n-1}\left(q_j+q_{j-1}\right)-\alpha\frac{\mathrm{De}}{1+\lambda}h_jq_{j-1/2}^{n-1}\left(u_j+u_{j-1}\right)\\&+\alpha\frac{\mathrm{De}}{1+\lambda}f_{j-1/2}^{n-1}\left(q_j-q_{j-1}\right)-\alpha\frac{\mathrm{De}}{1+\lambda}\frac{h_j}{2}\left(q'\right)_{j-1/2}^{n-1}\left(f_j+f_{j-1}\right)=\left[R_1\right]_{j-/12}^{n-1}\end{aligned} \tag{37}$$

$$\begin{aligned}&\left(1+\frac{K}{2}\right)\left(p_j-p_{j-1}\right)+\left(\frac{1}{2}+\alpha\right)\frac{h_j}{4}\left(f_j+f_{j-1}\right)\left(p_j+p_{j-1}\right)+\left(\frac{1}{2}-\alpha\right)\frac{h_j}{4}\left(u_j+u_{j-1}\right)\left(g_j+g_{j-1}\right)\\&-BK\xi\frac{h_j}{2}\left(2\left(g_j+g_{j-1}\right)+\left(v_j+v_{j-1}\right)\right)+\frac{\alpha h_j}{2}g_{j-1/2}^{n-1}\left(u_j+u_{j-1}\right)-\frac{\alpha h_j}{2}u_{j-1/2}^{n-1}\left(g_j+g_{j-1}\right)\\&-\frac{\alpha h_j}{2}f_{j-1/2}^{n-1}\left(p_j+p_{j-1}\right)+\frac{\alpha h_j}{2}p_{j-1/2}^{n-1}\left(f_j+f_{j-1}\right)=\left[R_2\right]_{j-1/2}^{n-1}\end{aligned} \tag{38}$$

$$\begin{aligned}&\frac{1}{\Pr}\left(t_j-t_{j-1}\right)+\left(\frac{1}{2}+\alpha\right)\frac{h_j}{4}\left(f_j+f_{j-1}\right)\left(t_j+t_{j-1}\right)-\frac{\alpha h_j}{4}\left(u_j+u_{j-1}\right)\left(s_j+s_{j-1}\right)\\&+\frac{\alpha h_j}{2}s_{j-1/2}^{n-1}\left(u_j+u_{j-1}\right)-\frac{\alpha h_j}{2}u_{j-1/2}^{n-1}\left(s_j+s_{j-1}\right)-\frac{\alpha h_j}{2}f_{j-1/2}^{n-1}\left(t_j+t_{j-1}\right)+\frac{\alpha h_j}{2}t_{j-1/2}^{n-1}\left(f_j+f_{j-1}\right)=\left[R_3\right]_{j-1/2}^{n-1}\end{aligned} \tag{39}$$

where we have used the below abbreviations:

$$\left[R_1\right]_{j-1/2}^{n-1}=-h_j\left[\begin{aligned}&\frac{(1+K)}{1+\lambda}(v')_{j-1/2}^{n-1}+\left(\frac{1}{2}-\alpha\right)(fv)_{j-1/2}^{n-1}+\alpha\left(u_{j-1}^{n-1}\right)^2-\frac{De}{1+\lambda}(uq)_{j-1/2}^{n-1}+Kp_{j-1/2}^{n-1}\\&-\frac{De}{1+\lambda}\left(\frac{1}{2}+\alpha\right)\left(v^2\right)_{j-1/2}^{n-1}-\frac{De}{1+\lambda}\left(\frac{1}{2}-\alpha\right)(fq')_{j-1}^{n-1}+R\xi\left[s_{j-1/2}^{n-1}+\alpha_1\left(s^2\right)_{j-1/2}^{n-1}\right]\end{aligned}\right] \tag{40}$$

$$\left[R_2\right]_{j-1/2}^{n-1}=-h_j\left[\left(1+\frac{K}{2}\right)(p')_{j-1/2}^{n-1}+\left(\frac{1}{2}-\alpha\right)(fp)_{j-1/2}^{n-1}+\left(\frac{1}{2}+\alpha\right)(ug)_{j-1/2}^{n-1}-KB\xi\left(2g_{j-1/2}^{n-1}+v_{j-1/2}^{n-1}\right)\right] \tag{41}$$

$$[R_3]_{j-1/2}^{n-1} = -h_j\left[\frac{1}{\Pr}(t')_{j-1/2}^{n-1} + \left(\frac{1}{2}-\alpha\right)(ft)_{j-1/2}^{n-1} + \alpha(us)_{j-1/2}^{n-1}\right] \tag{42}$$

The boundary conditions are:

$$f_0^n = u_0^n = 0, \quad s_0^n = 1, \quad g_0^n = 1, \quad u_J^n = 0, \quad v_J^n = 0, \quad s_J^n = 0, \quad g_0^n = 0 \tag{43}$$

Stage 3: Quasi-linearization of Non-Linear Keller Algebraic Equations

If we assume $f_j^{n-1}, u_j^{n-1}, v_j^{n-1}, q_j^{n-1}, g_j^{n-1}, p_j^{n-1}, s_j^{n-1}, t_j^{n-1}$ to be known for $0 \le j \le J$, this leads to a system of *8J+8* equations for the solution of *8J+8* unknowns $f_j^n, u_j^n, v_j^n, q_j^n, g_j^n, p_j^n, s_j^n, t_j^n$, $j = 0,1,2,\ldots,J$. This non-linear system of algebraic equations is linearized by means of Newton's method.

Table 1. Comparison of *Nu* for different values of *Ri* and *Pr*.

Ri	*Pr* = 0.72		*Pr* = 10		*Pr* = 100	
	Lloyd and Sparrow [52]	Present	Lloyd and Sparrow [52]	Present	Lloyd and Sparrow [52]	Present
0.0	0.2956	0.2958	0.7281	0.7283	1.5720	1.5724
0.01	0.2979	0.2980	0.7313	0.7315	1.5750	1.5753
0.04	0.3044	0.3046	0.7404	0.7406	1.5850	1.5851
0.1	0.3158	0.3160	0.7574	0.7576	1.6050	1.6052
0.4	0.3561	0.3563	0.8259	0.8261	1.6910	1.6912
1.0	0.4058	0.4060	0.9212	0.9213	1.8260	1.8262

Table 2. Values of C_f, *Nu* and *Wcs* for various values of *De*, λ, *Pr*, *K* and ξ (*Ri* = 0.5, *B* = 0.5, α_1 = 5.0, Ω = π/6)

De	λ	*K*	*Pr*	ξ = 1			ξ = 2			ξ = 3		
				C_f	*Nu*	*Wcs*	C_f	*Nu*	*Wcs*	C_f	*Nu*	*Wcs*
0.02				1.3132	0.7549	-0.0960	1.9195	0.8499	-0.4761	2.4558	0.9174	-1.2411
0.5				1.3032	0.7562	-0.0979	1.9050	0.8502	-0.4793	2.4420	0.9187	-1.2429
1	0.2			1.2985	0.7577	-0.0998	1.9013	0.8504	-0.4828	2.4409	0.9187	-1.2453
3				1.2886	0.7628	-0.1075	1.8950	0.8515	-0.4996	2.4424	0.9195	-1.2639
5				1.2807	0.7690	-0.1158	1.8881	0.8549	-0.5207	2.4399	0.9202	-1.2937
10		3.0		1.2595	0.7915	-0.1387	1.8631	0.8715	-0.5857	2.4186	0.9306	-1.4015
	0			1.3132	0.7549	-0.0960	1.9195	0.8499	-0.4761	2.4558	0.9174	-1.2411
	0.25			1.3032	0.7562	-0.0979	1.9050	0.8502	-0.4793	2.4420	0.9187	-1.2429
	0.5		7.0	1.2985	0.7577	-0.0998	1.9013	0.8504	-0.4828	2.4409	0.9187	-1.2453
	0.75			1.2886	0.7628	-0.1075	1.8950	0.8515	-0.4996	2.4424	0.9195	-1.2939
	1			1.2807	0.7690	-0.1158	1.8881	0.8549	-0.5207	2.4399	0.9202	-1.2937
	1.5			1.2595	0.7915	-0.1387	1.8631	0.8715	-0.5857	2.4186	0.9309	-1.4015
		0		1.1941	0.9714	0.0069	1.8119	1.1089	0.0157	2.3580	1.2053	0.0259
		0.5		1.1956	0.8995	-0.0616	1.8199	1.0241	-0.3094	2.3585	1.1124	-0.7953
0.1		1.0		1.2119	0.8523	-0.0872	1.8357	0.9681	-0.4284	2.3785	1.0512	-1.1005
		1.5		1.2397	0.8183	-0.0965	1.8438	0.8275	-0.4728	2.4017	1.0066	-1.2196
		2.0		1.2408	0.7924	-0.0984	1.8765	0.8961	-0.4861	2.4106	0.9718	-1.2586
	0.2	2.5		1.2734	0.7719	-0.0990	1.9330	0.8708	-0.4849	2.5459	0.9436	-1.2595
			0.5	1.9454	0.3507	-0.1939	2.9983	0.3968	-1.0266	3.9273	0.4301	-2.7326
			0.71	1.8660	0.3860	-0.1801	2.8501	0.4385	-0.9463	3.7203	0.4764	-2.5098
		3.0	2	1.5981	0.5226	-0.1379	2.3986	0.5936	-0.7088	3.1041	0.6454	-1.8667
			5	1.3818	0.6845	-0.1061	2.0346	0.7726	-0.5314	2.6122	0.8377	-1.3897
			7	1.3106	0.7551	-0.0964	1.9144	0.8498	-0.4766	2.4496	0.9200	-1.2415
			10	1.2400	0.8376	-0.0871	1.7949	0.9394	-0.4244	2.2880	1.0155	-1.0998

Stage 4: Block-tridiagonal Elimination

The linearized system is solved by the block-elimination method since it possesses a block-tridiagonal structure. The block-tridiagonal structure generated consists of *block matrices*. The complete linearized system is formulated as a *block matrix system*, where each element in the coefficient matrix is a matrix itself, and this system is solved using the efficient Keller-box method. The numerical results are strongly influenced by the number of mesh points in both directions. After some trials in the η-direction (radial coordinate), a larger number of mesh points are selected whereas in the ξ-direction (tangential coordinate) significantly less mesh points are utilized. $\eta_{\max}$ has been set at 12 and this defines an adequately

large value at which the prescribed boundary conditions are satisfied. ξ_{max} is set to 3.0 for this flow domain. Mesh independence is achieved in the present computations. The numerical algorithm is executed in MATLAB on a PC. The method demonstrates excellent stability, convergence and consistency, as elaborated by Keller [57].
To validate the Keller box numerical code employed, comparison with earlier Newtonian solutions presented by Lloyd and Sparrow [52] is conducted and shown in Table 1. Very close correlation is achieved for the Nusselt number (*Nu*) for different values of the mixed convection parameter (*R*) and three different values of Prandtl number (*Pr*) i.e. 0.72 (air), 10, 100 (polymers). Confidence in the present solutions is therefore very high.

5. Results and Discussion

Table 2 presents the numerical results of dimensionless skin friction (C_f), heat transfer rate (*Nu*) and wall couple stress (*Wcs*) for different values of *Deborah number, De, ratio of retardation to relaxation times, λ, Prandtl number, Pr and vortex viscosity, K* along with variations in stream-wise coordinate, ξ. An increasing *De* is observed to reduce C_f and *Wcs* whereas it increases *Nu*. Furthermore, an increase in λ reduces the skin friction wall couple stress but enhances heat transfer rate. Also, an increase in *K* is seen to reduce heat transfer rate and wall couple stress, but increases skin friction. Further, an increase in *Pr* reduces skin friction whereas it enhances heat transfer rate and wall couple stress.

Table 3 document results for the influence of *micro-inertia density parameter* (*B*), *angle of inclination* (Ω), *nonlinear temperature parameter* (α_1) and *mixed convection parameter* (*Ri*) on dimensionless skin friction, heat transfer rate and wall couple stress along with a variation in the traverse coordinate (ξ). Skin friction and wall couple stress is reduced with increasing *B* values however heat transfer rate is enhanced. Furthermore, the increasing values of Ω are seen to reduce skin friction and heat transfer rate whereas wall couple stress increases. Increasing *Ri* is seen to enhance skin friction, heat transfer rate but decreases wall couple stress. An increasing α_1, depresses the wall couple stress whereas elevates skin friction and heat transfer rate.

Table 3. Values of C_f, *Nu* and *Wcs* for various values of *B*, Ω, α_1, *Ri* and ξ (Pr = 7, De = 0.1, λ = 0.2, K = 3.0)

B	Ω	α_1	Ri	$\xi = 1$			$\xi = 2$			$\xi = 3$		
				C_f	Nu	Wcs	C_f	Nu	Wcs	C_f	Nu	Wcs
0				1.3638	0.7586	0.0151	1.9811	0.8474	0.0308	2.5298	0.9130	0.0467
1				1.2972	0.7578	-0.1684	1.8962	0.8555	-0.8352	2.4242	0.9275	-2.1724
2	π/6			1.2849	0.7629	-0.2853	1.8757	0.8636	-1.4213	2.3948	0.9376	-3.6797
5				1.2700	0.7729	-0.5474	1.8468	0.8773	-2.7339	2.3536	0.9538	-7.0217
10				1.2632	0.7828	-0.8617	1.8269	0.8888	-4.3173	23246	0.9667	-11.0417
	0	5.0		1.4135	0.7715	-0.1035	2.0901	0.8724	-0.5159	2.6883	0.9475	-1.3475
	π/6			1.3106	0.7551	-0.0964	1.9144	0.8498	-0.4766	2.4496	0.9200	-1.2415
	π/4			1.1842	0.7338	-0.0873	1.6976	0.8201	-0.4263	2.1548	0.8851	-1.1056
	π/3		0.5	1.0105	0.7024	-0.0743	1.3976	0.7750	-0.3526	1.7460	0.8314	-0.9057
	4π/9			0.7074	0.6395	-0.0793	0.8615	0.6775	-0.2052	1.0077	0.7104	-0.4990
	π/2			0.5217	0.5935	-0.0322	0.5119	0.5931	-0.0920	0.5082	0.5937	-0.1663
		0		0.7362	0.6539	-0.0557	0.9107	0.7013	-0.2433	1.0738	0.7412	-0.6033
		1		0.8627	0.6789	-0.0684	1.1364	0.7402	-0.301	1.3861	0.7894	-0.7633
0.5		3		1.0958	0.7206	-0.0821	1.5442	0.8014	-0.3968	1.9449	0.8631	-1.0252
		5		1.3106	0.7551	-0.0964	1.9144	0.8498	-0.4766	2.4496	0.9200	-1.2415
		7		1.5122	0.7848	-0.109	2.2594	0.8903	-0.5464	2.9188	0.9673	-1.4298
		10		1.7962	0.8231	-0.1258	2.7431	0.9416	-0.6381	3.5757	1.0265	-1.6769
	π/6		0	0.5217	0.5935	-0.0322	0.5119	0.5931	-0.0920	0.5082	0.5937	-0.1663
			0.35	1.1100	0.7191	-0.0812	1.5542	0.7992	-0.3917	1.9596	0.8603	-1.0120
			0.7	1.5707	0.7954	-0.1140	2.3578	0.9047	-0.5736	3.0516	0.9841	-1.5026
		5.0	1.05	1.9889	0.8529	-0.1401	3.0669	0.9808	-0.7154	4.0129	1.0716	-1.8839
			1.4	2.3744	0.8998	-0.1623	3.7185	1.0416	-0.8351	4.8961	1.1410	-2.2055
			2	2.9835	0.9655	-0.1947	4.7472	1.1254	-1.0085	6.2911	1.2358	-2.6721

Figs 3 - 26 illustrate graphical solutions for the influence of selected parameters on the velocity, temperature and angular velocity characteristics. Figs. 3 – 5 depict the influence of Deborah number, *De* (viscoelastic parameter) on velocity, temperature and angular velocity (f', θ and g). In all graphs, plate inclination is set at $\Omega = \pi/6$. Asymptotically smooth distributions are generally achieved in the freestream for all graphs indicating that a sufficiently large infinity boundary condition is specified in the Keller box numerical code. Fig. 3 shows the influence of *De* on f' and clearly increasing *De* (which corresponds to greater elastic effects to viscous effects) results in flow acceleration. *De* embodies the ratio of relaxation time it takes for the fluid to adjust to applied stresses or deformations and the characteristic time scale. Momentum boundary layer thickness is therefore reduced with increasing Deborah number. The fluid (polymer) behaves more like a viscous fluid at lower Deborah number whereas at higher Deborah numbers, the behavior is more influenced by elasticity. Fig. 4 demonstrates that increasing *De* values results in a decrease in temperature i.e. reduction in thermal boundary layer thickness. The effect of *De* on the angular velocity is shown in Fig. 5 and a significant reduction is observed i.e. it inhibits motion in micro-element rotary.

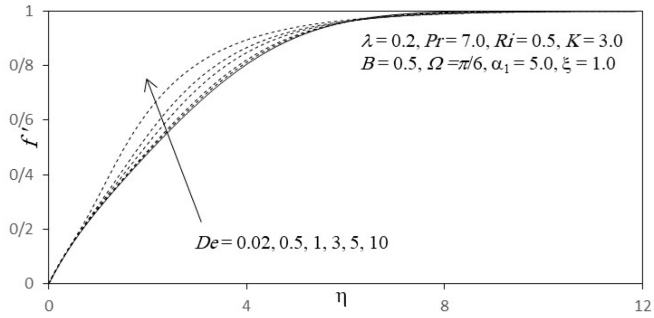

Fig. 3. Influence of *De* on velocity profiles

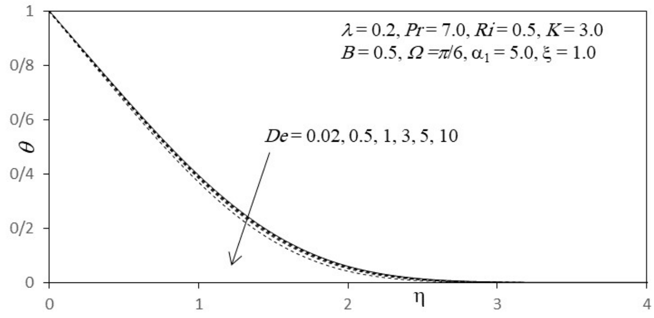

Fig. 4. Influence of *De* on temperature profiles

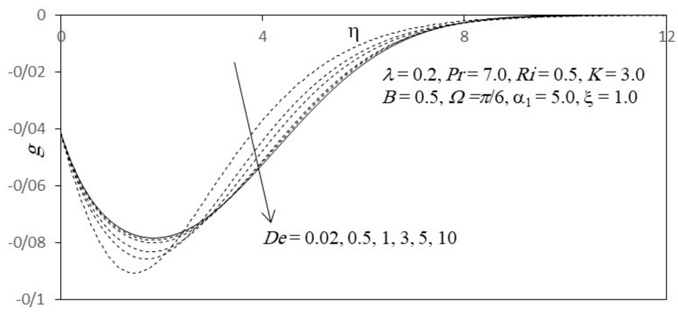

Fig. 5. Influence of *De* on angular velocity profiles

Figs. 6 – 8 show the response of fluid velocity (f'), temperature (θ) and angular velocity (g) with the ratio of relaxation to retardation times (λ). A significant elevation in velocity accompanies an increase in λ as observed in Fig. 5. Conversely, there is a strong reduction in temperature with increasing λ values (Fig. 7). Fig. 8 shows that angular velocity is reduced with increasing values λ, the micro-elements spin is encouraged. Effectively the rheology of Jeffery fluid has a marked influence on thermal and hydrodynamic characteristics. For the case of a Newtonian fluid (λ = 1), the results are noticeably different from the Jeffery case ($\lambda \neq 1$). When λ_1<1, the retardation time exceeds the relaxation time. This implies that the polymeric Jeffrey fluid responds faster with the removal of stress and returns quicker to its unperturbed state. The opposite behavior is the case when λ_1>1.

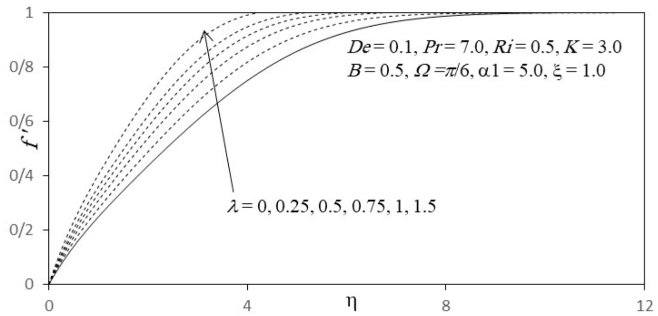

Fig. 6. Influence of λ on velocity profiles

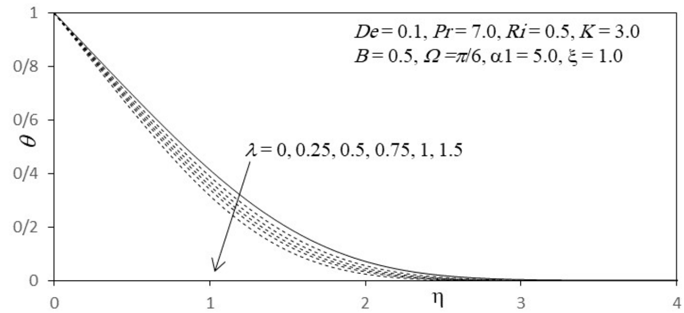

Fig. 7. Influence of λ on temperature profiles

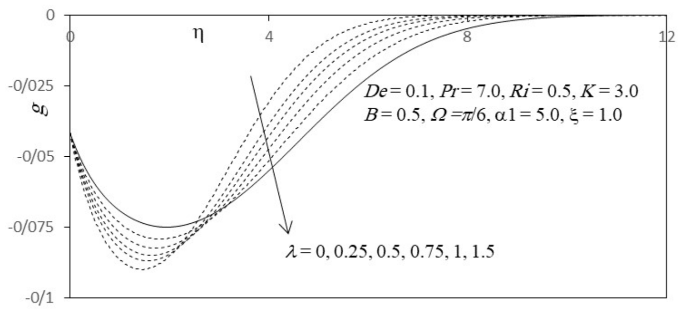

Fig. 8. Influence of λ on angular velocity profiles

Figs. 9 - 11 show the variations for velocity (f'), temperature (θ) and angular velocity (g) with different values of micropolar parameter (K). Fig. 9 indicates that an increase in K significantly reduces the boundary layer flow. And this trend is sustained throughout the boundary layer regime. The reverse spin is exhibited near the plate surface due to the microelements. Away from the wall, the micro-elements spin overwhelmingly accelerates the boundary layer flow. Hence, the linear momentum diffusion enhances [53]. In Fig. 10, we observe that the temperature profiles significantly elevated for greater values of K. Hence, the thermal boundary layer thickness is increased. The increase in K strengths the thermal diffusion and acts as an agitator. Thereby, the efficiency of thermal convection inside the fluid body is increased from microscopic to macroscopic scale and the heat is transported effectively with larger intensity from the surface of the plate into the fluid regime. In Fig. 11 a significant reduction in micro rotation is observed with an increase in K values. With increasing K values there is a progressive displacement in the peak for each micro rotation profile further away from the surface, this attributes to the greater facility for micro elements to rotate with greater space available. Hence, the micropolar fluids exhibit greater drag reducing properties compared to Newtonian fluids effectively. Generally, the heat transfer is also enhanced. The similar results were observed in the work of Gorla and Takhar [54] and Gorla *et al.* [55]. For K = 1 the micropolar and Newtonian dynamic viscosity are the same. And for K = 0, the micropolarity is ignored and the equations reduce to the Newtonian case. The parameter K has a prominent influence on all the flow variables.

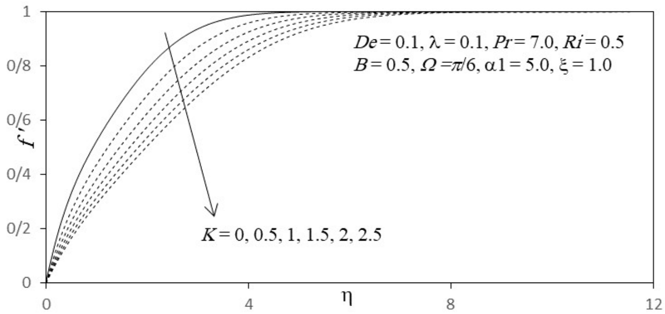

Fig. 9. Influence of K on velocity profiles

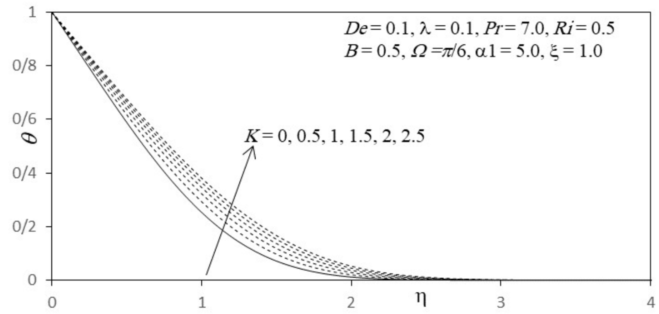

Fig. 10. Influence of K on temperature profiles

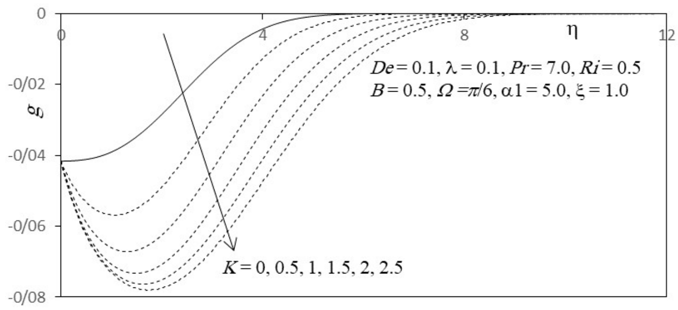

Fig. 11. Influence of K on angular velocity profiles

Figs. 12 – 14 present the influence of the micro-inertia density parameter (B) on velocity (f'), temperature (θ) and angular velocity (g). Fig. 12 indicates that an increase in B significantly increases the fluid velocity and is sustained throughout the boundary layer regime. Hence, the larger micro inertial density of the viscoelastic micropolar fluid enhances the flow. In Fig. 10, it is seen that the temperature profiles slightly decrease for greater values of B. In Fig. 11 a significant reduction in micro rotation is observed with greater B values. This is due to the larger micro inertial density associated with greater B values. The impact of this parameter on real flows has been elaborated by Eringen [29]. The similar results were observed in the work of Gorla and Takhar [54] and Gorla *et al.* [55].

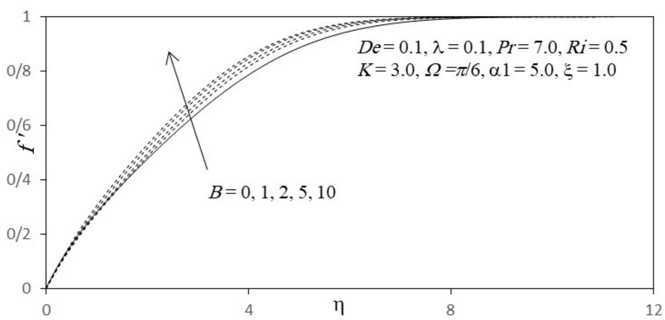

Fig. 12. Influence of B on velocity profiles

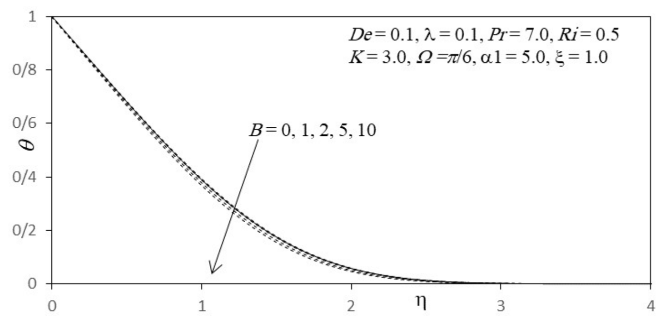

Fig. 13. Influence of B on temperature profiles

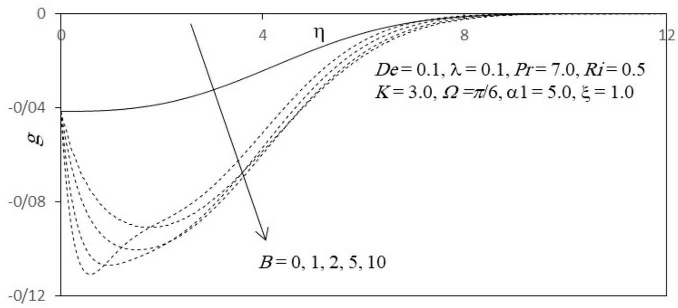

Fig. 14. Influence of B on angular velocity profiles

Figs. 15 – 17 depict the evolution in fluid velocity (f'), Jeffery fluid temperature (θ) and angular velocity (g) with a modification in stream-wise coordinate (ξ). Fig. 15 shows that increasing ξ raises the velocity magnitudes. The velocity is minimum at $\xi = 0$. The parameter ξ exerts a great impact on the momentum development. Conversely, temperature and angular velocity (Figs. 16 & 17) are significantly decelerated with increasing ξ. A monotonic deceleration in temperature and angular velocity is observed with a rise in ξ. Hence, the fluid is cooled and thermal boundary layer thickness decreases. The angular velocity is also seen to decelerate significantly for large values of ξ. The micro-rotation is stifled near the leading edge where the boundary layer begins to grow. The spatial capacity for gyratory motions is very restricted here and this induces reverse spin.

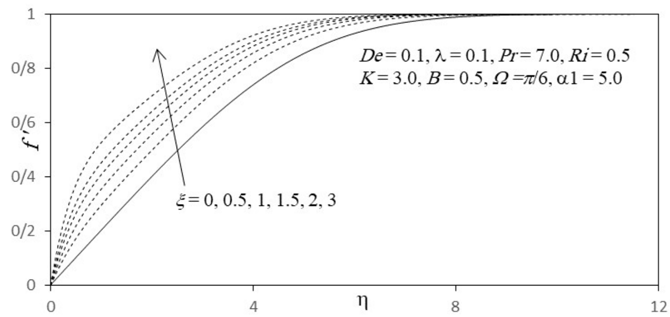

Fig. 15. Influence of ξ on velocity profiles

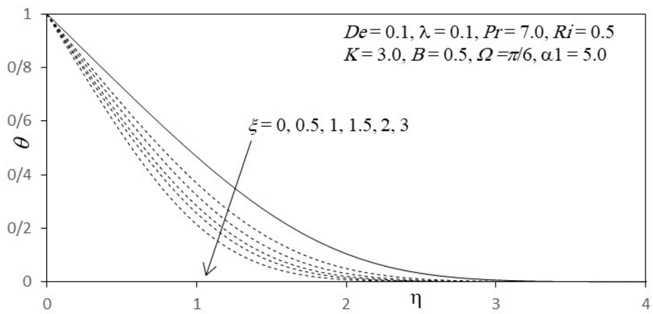

Fig. 16. Influence of ξ on temperature profiles

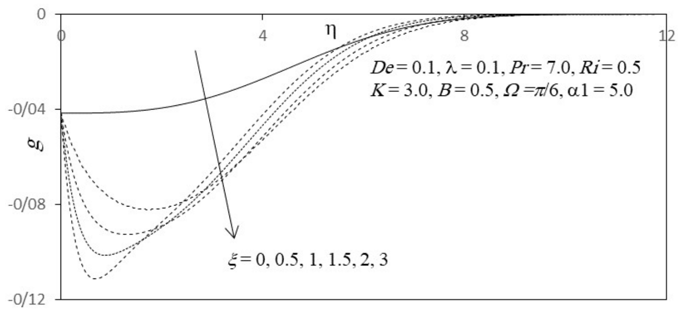

Fig. 17. Influence of ξ on angular velocity profiles

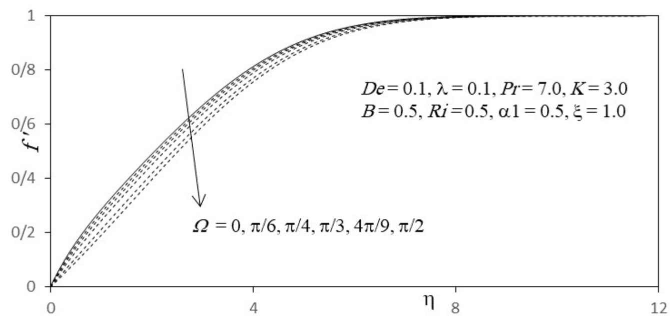

Fig. 18. Influence of Ω on velocity profiles

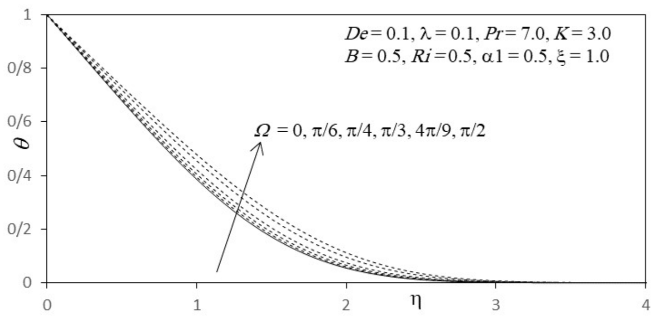

Fig. 19. Influence of Ω on temperature profiles

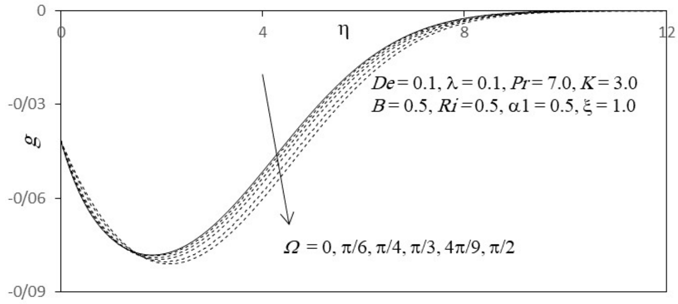

Fig. 20. Influence of Ω on angular velocity profiles

Figs. 18 – 20 show the distributions for velocity (f'), fluid temperature (θ) and angular velocity (g) with angle of inclination, Ω varying between 0^0 – 90^0. Fig. 18 indicates that a significant deceleration in the boundary layer flow is associated with Ω which is due to the reduction in the thermal buoyancy effect in Eq. (5). From Fig. 19 we also observe for $\Omega = 0^0$ (vertical plate) the temperature attains maximum buoyancy force. Increasing angle of inclination parameter (Ω) is observed in Fig. 19 to elevate the fluid temperature (θ) and enhances thermal boundary layer thickness. For vertical surface, it is observed that the temperature distributions are small but for horizontal surface they are large. Fig. 20 shows that angular velocity profiles decelerate with increasing inclination parameter i.e. as the plate position changes from vertical to horizontal, the angular velocity increases near the plate and a reverse trend is observed far away from the plate.

Figs. 21 – 23 visualize the response in fluid velocity (f'), Jeffery fluid temperature (θ) and angular velocity (g) to a variation in *mixed convection parameter* (*Ri*). Larger values of *Ri* correspond to stronger natural (free) convection i.e. greater Grashof numbers. A significant elevation in velocity is induced throughout the boundary layer transverse to the plate surface with increasing mixed convection parameter, *Ri*, as seen in Fig. 21. Momentum boundary layer thickness is therefore decreased. Temperatures are considerably depleted (Fig. 22) with greater *Ri* values i.e. thermal boundary layer thickness is reduced. In both Figs. 21 and 22 the trends are sustained throughout the boundary layer. Fig. 23 shows that in close proximity to the plate surface there is a significant increase in angular velocity with a rise in mixed convection parameter.

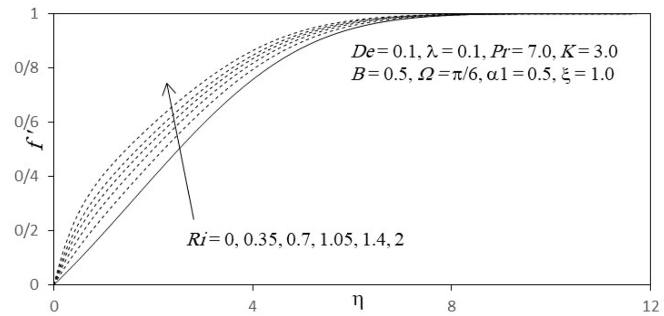

Fig. 21. Influence of *Ri* on velocity profiles

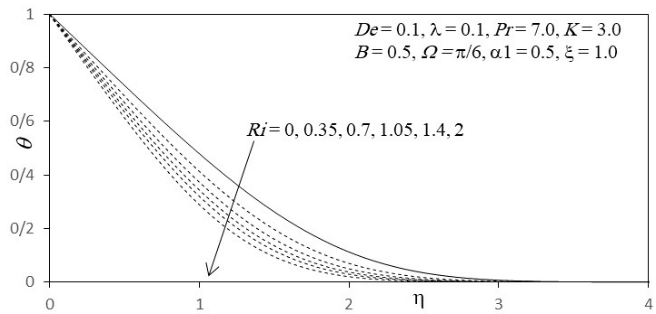

Fig. 22. Influence of *Ri* on temperature profiles

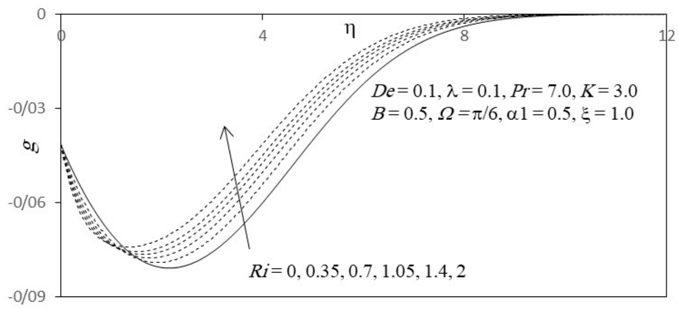

Fig. 23. Influence of *Ri* on angular velocity profiles

Figs. 24 – 26 show the distributions for velocity (f'), fluid temperature (θ) and angular velocity (g) with different values of *nonlinear temperature* (α_1). Fig. 24 indicates that a weak acceleration in the boundary layer flow is associated with a large rise in α_1. Increasing α_1 is observed in Fig. 25 to strongly decelerate the fluid temperature and thermal boundary layer thickness also reduced. Fig. 26 shows that angular velocity rises slightly.

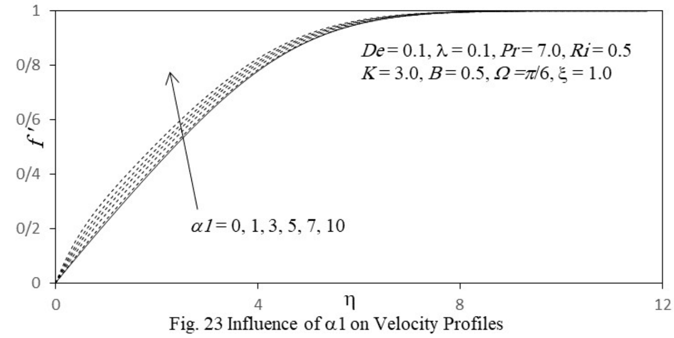

Fig. 24. Influence of $\alpha 1$ on velocity profiles

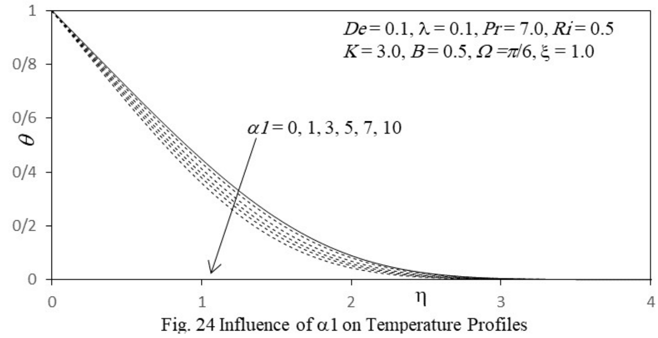

Fig. 25. Influence of $\alpha 1$ on temperature profiles

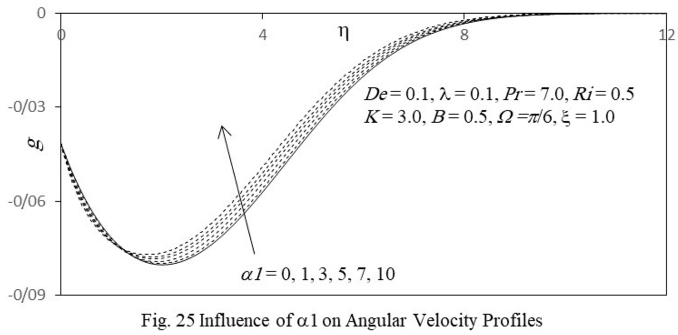

Fig. 26. Influence of $\alpha 1$ on angular velocity profiles

6. Conclusions

A mathematical model has been developed to simulate the steady-state natural convection boundary layer flow of an electrically-conducting viscoelastic fluid (polymer) from an inclined plate in Eringen micropolar fluid regime with nonlinear temperature. The governing conservation equations and associated wall and free stream boundary conditions have been transformed into a nonlinear dimensionless boundary value problem. The Jeffery elastic-viscous model has been used. The model has been developed to simulate non-Newtonian materials processing. An implicit finite difference scheme (Keller box method) has been implemented to solve the partial differential boundary value problem computationally. The main conclusions from the present study may be summarized as follows:

- Velocity is enhanced with increasing Deborah number, relaxation to retardation ratio, microinertia density parameter, stream-wise coordinate, mixed convection parameter and nonlinear temperature parameter whereas it is decreased with increasing angle of inclination and vortex viscosity parameter.
- Temperature is reduced with increasing Deborah number, relaxation to retardation ratio, mixed convection parameter, microinertia density parameter, stream-wise coordinate and nonlinear temperature whereas it is elevated with increasing vortex viscosity parameter and angle of inclination.
- Angular velocity is decreased with increasing Deborah number, relaxation to retardation ratio, vortex viscosity parameter, stream-wise coordinate, microinertia density parameter and angle of inclination whereas it is increased with increasing mixed convection parameter and nonlinear temperature.

The present study has ignored transient effects. These will be considered in the future in addition to alternative rheological models e.g. Oldroyd-B fluid model [56], which is also relevant to thermal polymer processing.

Nomenclature

B	Micropolar inertia density parameter	x	Stream wise coordinate
C_f	Skin Friction Coefficient	y	Transverse coordinate
c_p	Specific heat		***Greek Symbols***
De	Deborah Number	γ	Spin gradient viscosity
f	Dimensionless stream function	α	Thermal diffusivity
g	Dimensionless microrotation function	β	Coefficient of thermal expansion
g_1	Gravitational acceleration	λ	Ratio of relaxation to retardation times
Gr	Thermal Grashof number	λ_1	Retardation time
j	Microinertial density	η	Non-dimensional transverse coordinate
K	Vortex viscosity parameter	σ	Electric conductivity of the fluid
k	Thermal conductivity	Ω	Angle of inclination
L	Characteristic length	μ	Dynamic viscosity
M_w	Dimensionless wall couple stress	ξ	Non-dimensional tangential coordinate

N	Angular velocity	ν	Kinematic viscosity
Nu	Heat transfer coefficient (Local Nusselt number)	θ	Dimensionless temperature
Pr	Prandtl number	ρ	Fluid density
Ri	Mixed convection parameter	ξ	Dimensionless tangential coordinate
Re	Reynolds number	ψ	Non-dimensional stream function
S	Cauchy stress tensor		***Subscripts***
T	Fluid temperature	w	Conditions on the wall
V	Velocity vector	∞	Free stream condition
u, v	Dimensionless velocity components in X and Y direction respectively		

Conflict of Interest

The authors declared no potential conflicts of interest with respect to the research, authorship and publication of this article.

Funding

The authors received no financial support for the research, authorship and publication of this article.

References

[1] X. Huang, M.J. Gollner, Correlations for evaluation of flame spread over an inclined fuel surface, *Fire Safety Science,* 11 (2014) 222-233.
[2] P. Cheng, Film condensation along an inclined surface in a porous medium, *International Journal of Heat and Mass Transfer,* 24 (1981) 983-990.
[3] O. Anwar Bég, J. Zueco, T.B. Chang, Numerical analysis of hydromagnetic gravity-driven thin film micropolar flow along an inclined plane, *Chemical Engineering Communications,* 198(3) (2010) 312- 331.
[4] N.J. Balmforth *et al.,* Viscoplastic flow over an inclined surface, *Journal of Non-Newtonian Fluid Mechanics,* 142 (2007) 219-243.
[5] M.B. Ashraf *et al.,* Radiative mixed convection flow of an Oldroyd-B fluid over an inclined stretching surface, *Journal of Applied Mechanics and Technical Physics,* 57 (2016) 317–325.
[6] K. Pruess, Y. Zhang, A hybrid semi-analytical and numerical method for modeling wellbore heat transmission, *Proc. 30th Workshop on Geothermal Reservoir Engineering, Stanford University, Stanford, California, USA*, 2005.
[7] Y. Greener, S. Middleman, Blade-coating of a viscoelastic fluid, *Polymer Engineering and Science,* 14 (1974) 791-796.
[8] H.-C. Chang, E.A. Demekhin, *Complex Wave Dynamics on Thin Films*, Elsevier, Amsterdam, 2002.
[9] A.F. Johnson, Rheology of thermoplastic composites I, *Composites Manufacturing*, 6 (1995) 153-160.
[10] M.R. Ilias, N.A. Rawi, Steady aligned MHD free convection of Ferrofluids flow over an inclined plate, *Journal of Mechanical Engineering*, 14(2) (2017) 1-15.
[11] R. Kandasamy, N.A. bt Adnan, J.A. Abbas Abbood, M. Kamarulzaki, M. Saifullah, Electric field strength on water based aluminum alloys nanofluids flow up a non-linear inclined sheet, *Engineering Science and Technology, An International Journal*, 22(1) (2019) 229-236.
[12] I. Khan, S. Fatima, M.Y. Malik, T. Salahuddin, Exponentially varying viscosity of magnetohydrodynamic mixed convection Eyring-Powell nanofluid flow over an inclined surface, *Results in Physics*, 8 (2018) 1194-1203.
[13] D.V.V. Krishna Prasad, G.S. Krishna Chaitanya, R. Srinivasa Raju, Thermal diffusion effect on MHD mixed convection flow along a vertically inclined plate: A Casson fluid flow, *AIP Conference Proceedings*, 1953 (2018) 140089.
[14] MD. Shamshuddin, S.R. Mishra, T. Thumma, Chemically Reacting Radiative Casson Fluid over an inclined porous plate: A Numerical Study, *Numerical Heat Transfer and Fluid Flow, Lecture Notes in Mechanical Engineering*, (2019) 469-479.
[15] Ch. RamReddy, P. Naveen, D. Srinivasacharya, Influence of Non-linear Boussinesq Approximation on Natural Convective Flow of a Power-Law Fluid along an Inclined Plate under Convective Thermal Boundary Condition, *Nonlinear Engineering*, 8(1) (2019) 94–106.
[16] P. Rana, R. Bhargava, O.A. Beg, Numerical solution for mixed convection boundary layer flow of a nanofluid along an inclined plate embedded in a porous medium, *Computers and Mathematics with Applications*, 61 (2012) 25816-2832.
[17] M. Ramzan, M. Bilal, J.D. Chung, Effects of MHD homogeneous-hetrogeneous reactions on third grade fluid with Cateneo-Christov heat flux, *Journal of Molecular Liquids*, 223 (2016) 1284-1290.
[18] M. Ramzan, M. Bilal, J.D. Chung, MHD stagnation point Cattaneo–Christov heat flux in Williamson fluid flow with homogeneous–heterogeneous reactions and convective boundary condition—A numerical approach, *Journal of Molecular Liquids*, 225 (2017) 856-862.
[19] M. Ramzan, M. Bilal, J.D. Chung, Influence of homogeneous-heterogeneous reactions on MHD 3D Maxwell fluid flow with Cattaneo-Christov heat flux and convective boundary condition, *Journal of Molecular Liquids*, 230 (2017) 415-422.
[20] M. Ramzan, M. Bilal, J.D. Chung, Radiative flow of Powell-Eyring magneto-nanofluid over a stretching cylinder with chemical reaction and double stratification near a stagnation point, *PLoS ONE*, 12(1) (2017) e170790.
[21] M. Ramzan, M. Bilal, J.D. Chung, Soret and Dufour effects on three dimensional Upper-Convected Maxwell fluid

with chemical reaction and non-Linear radiative heat flux, *International Journal of Chemical Reactor Engineering*, 15(3) (2017) 20160136.
[22] M. Ramzan, M. Bilal, S. Kanwal, Effects of variable thermal conductivity and nonlinear thermal radiative flow past Eyring Powell nanofluid with chemical reaction, *Communications in Theoretical Physics*, 67(6) (2017) 723.
[23] M. Ramzan, M. Bilal, J.D. Chung, Radiative Williamson nanofluid flow over a convectively heated Riga plate with chemical reaction-A numerical approach, *Chinese Journal of Physics*, 55(4) (2017) 1663-1673.
[24] M.D. Shamshuddin, P.V. Satya Narayana, Primary and Secondary flows on unsteady MHD free convective micropolar fluid flow past an inclined plate in a rotating system: a Finite Element Analysis, *Fluid Dynamics and Materials Processing,* 14(1) (2018) 57-86.
[25] N. Manzoor, K. Maqbool, O.A. Bég, S. Shaheen, Adomian decomposition solution for propulsion of dissipative magnetic Jeffrey biofluid in a ciliated channel containing a porous medium with forced convection heat transfer, *Heat Transfer - Asian Research*, 48(2) (2019) 556-581.
[26] V.R. Prasad, S. Abdul Gaffar, E. Keshava Reddy, O. Anwar Bég, Numerical study of non-Newtonian boundary layer flow of Jeffreys fluid past a vertical porous plate in a non-Darcy porous medium, *Internatioanl Journal of Computer Mathematics, Engineering Science & Mechanics,* 15(4) (2014) 372-389.
[27] S. Abdul Gaffar, V. Ramachandra Prasad, O. Anwar Bég, Md. Hidayathullah Khan, K. Venkatadri, Effects of ramped wall temperature and concentration on viscoelastic Jeffrey's fluid flows from a vertical permeable cone, *Journal of the Brazilian Society of Mechanical Sciences and Engineering*, 40 (2018) 441-459.
[28] K. Ahmad, A. Ishak, Magnetohydrodynamic (MHD) Jeffrey fluid over a stretching vertical surface in a porous medium, *Propulsion and Power Research,* 6(4) (2017) 269-276.
[29] A.C. Eringen, Simple microfluids, *International Journal of Engineering Science*, 2 (1964) 205-217.
[30] A.C. Eringen, Theory of micropolar fluids, *Journal of Mathematics & Mechanics,* 16 (1966) 1-18.
[31] A.C. Eringen, Theory of thermo-micropolar fluids, *Journal of Mathematical Analysis Applications*, 38 (1972) 480–496.
[32] S.R. Mishra, M. Mainul Hoque, B. Mohanty, N.N. Anika, Heat transfer effect on MHD flow of a micropolar fluid through porous medium with uniform heat source and radiation, *Nonlinear Engineering*, 8(1) (2019) 65–73.
[33] I. Pazanin, M. Radulovic, Asymptotic Approximation of the nonsteady Micropolar fluid flow through a circular pipe, *Mathematical Problems in Engineering*, 2018 (2018) Article ID 6759876, 16p.
[34] M. Nazeer, N. Ali, T. Javed, Z. Asghar, Natural convection through spherical particles of a micropolar fluid enclosed in a trapezoidal porous container, *The European Physical Journal Plus*, 133 (2018) 423.
[35] O.K. Koriko, I.L. Animasaun, A.J. Omowaye, T. Oreyeni, The combined influence of nonlinear thermal radiation and thermal stratification on the dynamics of micropolar fluid along a vertical surface, *Multidiscipline Modeling in Materials and Structures,* 15(1) (2019) 133-155.
[36] R. Mehmood, S. Nadeem, S. Masood, Effects of transverse magnetic field on a rotating micropolar fluid between parallel plates with heat transfer, *Journal of Magnetism and Magnetic Materials,* 401 (2016) 1006-1014.
[37] M. Ramzan, J.D. Chung, N. Ullah, Partial slip effect in the flow of MHD micropolar nanofluid flow due to a roztating disk – A numerical approach, *Results in Physics*, 7 (2017) 3557-3566.
[38] M. Ramzan, N. Ullah, J.D. Chung, D. Lu, U. Farooq, Buoyancy effects on the radiative magneto Micropolar nanofluid flow with double stratification, activation energy and binary chemical reaction, *Scientific Reports*, 7 (2017) 12901.
[39] A. Maceiras, P. Martins, High-temperature polymer based magnetoelectric nanocomposites, *European Polymer Journal*, 64 (2015) 224-228.
[40] P.M. Xulu, P. Filipcsei, M. Zrinyi, Preparation and responsive properties of magnetically soft poly (*N*-isopropylacrylamide) gels, *Macromolecules,* 33(5) (2000) 1716-1719.
[41] O.A. Bég, Numerical methods for multi-physical magnetohydrodynamics, *New Developments in Hydrodynamics Research, M. J. Ibragimov and M. A. Anisimov, Eds.*, *Nova Science, New York, September,* 2012, p 1-112.
[42] S. Abdul Gaffar, V. Ramachandra Prasad E. Keshava Reddy, MHD free convection flow of non-Newtonian Eyring-Powell fluid from vertical surface in porous media with Hall/Ionslip currents and Ohmic dissipation, *Alexandria Engineering Journal,* 55 (2016) 875-905.
[43] S. Abdul Gaffar, V. Ramachandra Prasad, E. Keshava Reddy, Computational Study of MHD free convection flow of non-Newtonian Tangent Hyperbolic fluid from a vertical surface in porous media with Hall/Ionslip current and Ohmic dissipation, *International Journal of Applied and Computational Mathematics*, 3(2) (2017) 859-890.
[44] O.A.Beg, S. Abdul Gaffar, V. Ramachandra Prasad, M.J. Uddin, Computational solutions for non-isothermal, nonlinear magneto-convection in porous media with hall/ionslip currents and ohmic dissipation, *Engineering Science and Technology, An International Journal,* 19(1) (2016) 377-394.
[45] M.T. Shaw, *Introduction to Polymer Rheology*, Wiley, New York, 2012.
[46] O.A. Bég, R. Bhargava, M.M. Rashidi, Numerical Simulation in Micropolar Fluid Dynamics, Lambert, Saarbrucken, Germany, 2011.
[47] O.A. Bég, V. R. Prasad, B. Vasu, N. Bhaskar Reddy, Q. Li, R. Bhargava, Free convection heat and mass transfer from an isothermal sphere to a micropolar regime with Soret/Dufour effects, *International Journal of Heat and Mass Transfer*, 54 (2011) 9-18.
[48] S. Abdul Gaffar, O.A. Bég, V. R. Prasad, Mathematical modelling of natural convection in a third grade viscoelastic

micropolar fluid from an isothermal inverted cone, *Iranian Journal of Science and Technology Transactions of Mechanical Engineering,* (2018) https://doi.org/10.1007/s40997-018-0262-x.
[49] A. Subba Rao, Prasad, V.R., O.A. Bég, Rashidi, M., Free convection heat and mass transfer of a nanofluid past a horizontal cylinder embedded in a non-Darcy porous medium, *Journal of Porous Media,* 21(3) (2018) 279-294.
[50] B. Vasu, Rama S. R. Gorla, O.A. Bég, P.V.S. N. Murthy, V.R. Prasad, A. Kadir, Unsteady flow of a nanofluid over a sphere with non-linear Boussinesq approximation, *AIAA Journal of Thermophysics Heat Transfer*, (2018) 13p. https://doi.org/10.2514/1.T5516.
[51] S.A. Gaffar, V.R. Prasad, B.R. Kumar, O.A. Bég, Computational modelling and solutions for mixed convection boundary layer flows of nanofluid from a non-isothermal wedge, *Journal of Nanofluids*, 7 (2018) 1-9.
[52] J.R. Lloyd, E.M., Sparrow, Combined forced and free convection flow on vertical surfaces. *International Journal Heat Mass Transfer*, 13(2) (1970) 434-438.
[53] S.G. Rochelle, J. Peddieson, Viscoelastic boundary-layer flows past wedges and cones, *International Journal of Engineering Science*, 18 (1980) 713–726.
[54] R.S.R. Gorla, H.S. Takhar, Boundary layer flow of micropolar fluid on rotating axisymmetric surfaces with a concentrated heat source, *Acta Mechanica*, 105 (1994) 1–10.
[55] R.S.R. Gorla, A. Slaouti, H.S. Takhar, Free convection in micropolar fluids over a uniformly heated vertical plate, *International Journal of Numerical Methods for Heat & Fluid Flow*, 8 (1988) 504-518.
[56] M. Norouzi, M. Davoodi, O.A. Bég, MD. Shamshuddin, Theoretical study of Oldroyd-B visco-elastic fluid flow through curved pipes with slip effects in polymer flow processing, *International Journal of Applied Computational Mathematics,* 4 (2018) 108.
[57] H.B. Keller, Numerical methods in boundary-layer theory, *Annual Review of Fluid Mechanics*, 10 (1978) 417-433.

ORCID iD

S. Abdul Gaffar http://orcid.org/0000-0002-7368-1658
P. Ramesh Reddy http://orcid.org/0000-0002-6666-7444
V. Ramachandra Pradesh http://orcid.org/0000-0002-9168-3825
A. Subba Rao http://orcid.org/0000-0001-8740-3862
B. Md. Hidayathulla Khan http://orcid.org/0000-0002-0310-8020